Am J Transl Res 2022;14(11):8009-8022
www.ajtr.org /ISSN:1943-8141/AJTR0144720

Original Article

Immunological classification of glioblastoma and its prognostic implications

Qiangwei Wang[1,2,3], Weiwei Lin[1,2], Tianjian Liu[1,2], Jue Hu[4], Yongjian Zhu[1,2]

[1]Department of Neurosurgery, The Second Affiliated Hospital, Zhejiang University School of Medicine, Hangzhou 310009, Zhejiang, China; [2]Clinical Research Center for Neurological Diseases of Zhejiang Province, Hangzhou 310009, Zhejiang, China; [3]Chinese Glioma Genome Atlas Network (CGGA) and Asian Glioma Genome Atlas Network (AGGA), Beijing 100070, China; [4]School of Basic Medical Sciences and Forensic Medicine, Hangzhou Medical College, Hangzhou 311399, Zhejiang, China

Received June 13, 2022; Accepted September 27, 2022; Epub November 15, 2022; Published November 30, 2022

Abstract: Objectives: The progress of immunotherapy for glioblastoma (GBM) is currently slow. To improve immunotherapy, we need a deeper understanding of the immune microenvironment of GBM. Here, we aimed to establish a classification system based on immune expression profile in GBM. Methods: Immune gene expression profiles of 152 patients with GBM from The Cancer Genome Atlas (TCGA) were used to identify subtypes by consensus clustering, and the classification system was reproduced in the two validation datasets (CGGA and GSE16011). Clinical information, molecular characteristics, immune infiltration, and genomic variation were integrated to characterize the subtypes. Results: Two distinct immune subtypes in GBM were successfully identified and validated. The Im2 subtype was closely related to *IDH*-wildtype and combined +7/-10, while the Im1 subtype was associated with *IDH* mutation. Survival curve analysis showed that the Im2 subtype was associated with significantly shorter survival than the Im1 subtype. Im2 showed a high immune score and stromal score, low tumor purity, enrichment of macrophages, and high immune checkpoint and *HLA* gene expression. Im1 was characterized by low immune score and stromal score, high tumor purity, enrichment of lymphocytes, and low immune checkpoint and *HLA* gene expression. Finally, we developed an immune-related signature in GBM with better prognosis prediction. Conclusions: Our study confirmed the immune heterogeneity of GBM and might provide valuable classification for immunotherapy.

Keywords: Glioblastoma, immune classification, survival, tumor immunity

Introduction

Glioblastoma (GBM) is the most common primary malignant tumor of the central nervous system [1, 2]. As the most aggressive glioma, GBM (WHO grade 4) accounts for 57% of all gliomas [3]. The standard treatment for GBM includes maximal surgical resection and postoperative combined radiotherapy and temozolomide (TMZ), followed by six cycles of adjuvant chemotherapy with TMZ. Despite standardized treatment, GBM patients have a poor overall prognosis with a median survival of 14.6 months [4, 5]. The prognosis of GBM has not made great progress in recent years, primarily because of the aggressive growth of tumor cells, protection by the blood-brain barrier, and the lack of key carcinogenic pathways for targeted therapy [6].

To improve outcomes for GBM patients, massive efforts have been made to explore better treatment options, such as immunotherapy. Currently, clinical trials of immunotherapy in GBM patients mainly include immune checkpoint blockade, vaccination, chimeric antigen receptor (CAR) T cells, and oncolytic viruses [7]. Vaccines are one of the most promising approaches, although some phase II and III trials have yielded no positive results [8, 9]. Despite the biological activity of many vaccines, low levels of immune stimulation are not sufficient to improve patient outcomes. CAR-T cells have been shown to be effective in treating hematologic tumors, but failed to improve outcome of GBM in a recent trial [10]. Immune checkpoint blockade showed promising therapeutic response in a GBM preclinical study [11, 12], but the current phase III clinical trials

for GBM have been unsuccessful [13-15]. Infection with oncolytic virus not only directly kills tumor cells but also triggers a broad antitumor immune response [16]. However, the clinical benefits of oncolytic virus for GBM are still limited [17]. The current status of immunotherapy in GBM is uncertain. The mechanisms of immunotherapy resistance in GBM include molecular heterogeneity, systemic immunosuppression, adaptive resistance, and reprogramming of myeloid cells [18].

To improve the efficacy of immunotherapy for GBM, a deep understanding of the immune microenvironment and its underlying mechanisms are needed. In the present study, we divided GBM into two immune subtypes based on immune-related genes. These two immune subtypes showed distinct clinical, molecular, prognostic, and immune characteristics. Our study revealed the immune heterogeneity in GBM, and our classification might have clinical implications to facilitate the precise immunotherapy for GBM.

Methods

GBM patient acquisition

Our study collected a total of 450 patients with GBM from The Cancer Genome Atlas (TCGA), Chinese Glioma Genome Atlas (CGGA), and GSE16011. For TCGA dataset (152 GBM patients), we collected the RNA-seq data, clinical and molecular information, somatic mutation and copy-number alterations (CNAs) (http://cancergenome.nih.gov/). Measures of DNA damage, including copy number variation burden, aneuploidy score, homologous recombination deficiency, and intratumoral heterogeneity were also retrieved [19]. Two validation datasets included RNA-seq data of 139 GBMs from the CGGA dataset [20] and RNA microarray data of 159 GBMs from the GSE16011 dataset [21]. Clinical and molecular information was also collected from two validation datasets. This study was approved by the hospital ethics committee and conducted in accordance with the Declaration of Helsinki. Informed consents from participants existed in the three datasets [22].

Identification of immune subtypes

Using 771 immune-related genes [23], we first performed univariate Cox regression analysis in TCGA dataset to screen out the genes associated with prognosis. Next, consensus clustering (R package "ConsensusClusterPlus") was performed with the candidate genes (Median Absolute Deviation, MAD > 0.5) to identify immune subtypes of TCGA patients. The maximum value of K was 10.

To predict immune subtypes in the CGGA and GSE16011 datasets, a partition around medoids (PAM) classifier was trained with TCGA dataset (R package "pamr"). Each patient was classified into an immune subtype based on the correlation with the centroid. Reproducibility and similarity of immune subtypes between training and validation datasets were assessed using the in-group proportion (IGP) statistics.

Evaluation of immune infiltration

Immune fraction, stromal fraction, and tumor purity were calculated using the ESTIMATE algorithm [24]. The CIBERSORT algorithm calculated the proportion of 22 types of immune cells infiltrating the tumor [25]. Enrichment levels of 29 immune signatures [26] were determined by single sample Gene Set Enrichment Analysis (ssGSEA, R package "GSVA").

Development of an immune-related signature

We screened the differentially expressed genes (fold change > 2 or < 0.5, FDR < 0.05) between the two immune subtypes in the TCGA dataset. Then, univariate Cox regression analysis was performed to identify genes with prognostic significance ($P < 0.05$, Wald test). Next, we selected the genes shared by all three datasets as candidate genes. Finally, an optimal Cox proportional hazard model (26 genes) was constructed using the Least Absolute Shrinkage and Selection Operator (LASSO) algorithm. Our immune-related signature was developed with a linear combination of 26 gene expression level (expr) weighted by LASSO regression coefficients: Risk Score = $(expr_{gene1} \times coefficient_{gene1}) + (expr_{gene2} \times coefficient_{gene2}) + \ldots + (expr_{gene26} \times coefficient_{gene26})$.

Bioinformatic analysis

Expression patterns of two immune subtypes were evaluated by principal component analysis (PCA) with R package "gmodels". Up-regulated and down-regulated genes in the Im2 subtype were selected for Gene Ontology (GO) analysis in DAVID Bioinformatics Resources

6.8 [27]. Gene set enrichment analysis (GSEA) was performed with R package "fgsea". The Tumor Immune Dysfunction and Exclusion (TIDE) score was calculated to predict patient response to immune checkpoint blockade [28]. Time-dependent ROC curve (timeROC) was used to predict the overall survival of patients at 1, 2, and 3 years [29].

Immunohistochemical staining

Formalin-fixed, paraffin-embedded GBM specimens were cut (5 μm section), deparaffinized, and rehydrated before antigen repair in buffer specified by the manufacturer. After blocking endogenous peroxidase activity with ethanol containing 3% hydrogen peroxidase, we incubated sections in primary antibody overnight at 4°C, followed with secondary antibodies (anti-mouse or anti-rabbit). In this study, our stained sections were scored by two experienced pathologists. The staining intensity was 0-3 points: 0 (negative), 1 (weak), 2 (moderate), and 3 (strong). The extent of staining reflected the percentage of positive cells: 0 (< 5%), 1 (6%-25%), 2 (26%-50%), 3 (51%-75%), and 4 (> 75%). Staining index was defined as the product of staining intensity and staining extent. For each primary antibody, we did preliminary experiment. We selected two times, equal to, or half of the recommended dilution concentration for the experiment, and the best results of positive expression were used for the formal experiment.

Statistical analysis

R language (https://www.r-project.org/) was used for most statistical analysis. Differences between immune subtypes were verified using Student's *t*-test or chi-square test. Differences in survival by Kaplan-Meier analysis were assessed using the log-rank test. In addition, the R packages involving drawing also included pheatmap, gglpot2, Hmisc, and ComplexHeatmap. A two-sided *p-value* < 0.05 was considered significant.

Results

Identification of two immune subtypes in glioblastomas

To reveal the immune heterogeneity in GBM, we performed cluster analysis with 771 immune genes in the literature [23]. The workflow is shown in **Figure 1A**. We screened 99 prognosis-related genes by Cox regression analysis (P < 0.05, Wald test). By performing consensus clustering on expression profiles of candidate genes (MAD > 0.5), we identified two robust immune subtypes, Im1 and Im2 (**Figures 1B** and S1). Then PCA analysis based on the immune candidate genes showed a different distribution pattern between the two subtypes (**Figure 1C**). Moreover, survival curve analysis showed that Im2 was associated with significantly shorter survival than Im1 (P = 0.013, **Figure 1D**).

To validate the above results, we used the TCGA dataset to train a Partition Around Medoids (PAM) classifier to predict the immune subtypes of patients in the CGGA and GSE16011 datasets. Each patient in the validation dataset was classified into a subtype based on the correlation with the centroid (**Figure 1B**) [30]. In-group-proportion (IGP) analysis revealed that the subtypes of the training and validation datasets were highly consistent (Table S1). Additionally, the two immune subtypes obtained in validation datasets showed a similar expression distribution pattern and survival characteristics with the TCGA dataset (**Figure 1C**, **1D**).

Clinical and molecular features of two immune subtypes

Next, we further analyzed the clinical characteristics of the two immune subtypes. There were significantly more patients over the age of 45 years in Im2 than in Im1 (P < 0.05, **Figure 2A**; Table S2). IDH-wildtype, combined gain of entire chromosome 7 and loss of entire chromosome 10 (combined +7/-10), was significantly associated with Im2 (P < 0.05). Then, our immune classification was compared with the previous TCGA transcriptome and methylation classification [31, 32]. We found that the TCGA subtype mesenchymal and methylation clusters LGm5 were significantly enriched in Im2 (P < 0.05). Im1 was associated with TCGA subtype proneural and LGm1 (P < 0.05). We observed similar clinical and molecular characteristics in the two validation datasets (**Figure 2B** and **2C**; Tables S3 and S4).

Functional annotation of immune subtypes

To characterize two immune subtypes, we screened for differentially expressed genes (DEGs) (fold change > 2 or < 0.5, FDR < 0.05,

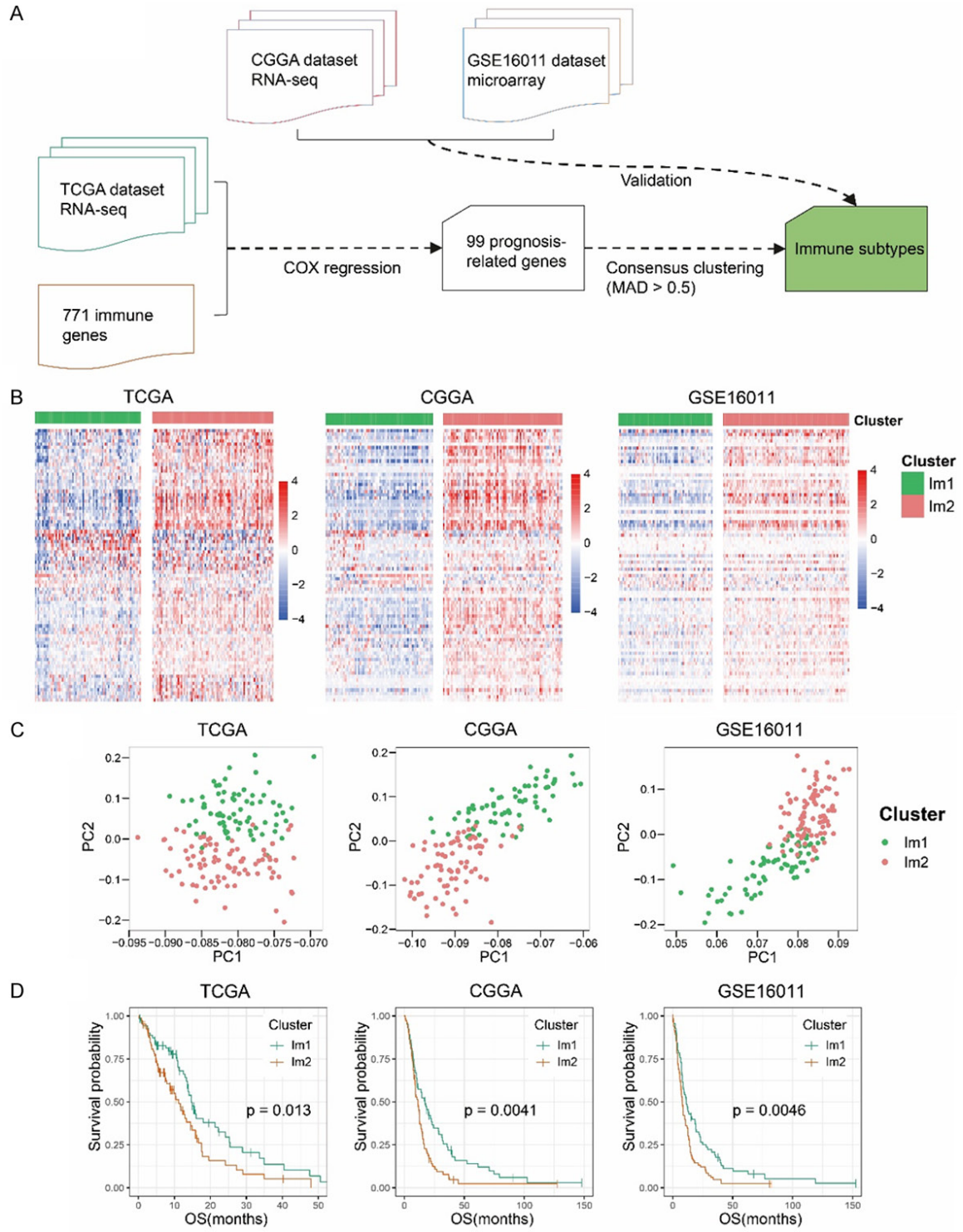

Figure 1. Identification of two subtypes in GBM through immune gene profiling. A. The flow chart shows how to identify and validate the two immune subtypes. B. Heatmaps of two immune subtypes from three databases. C. Principal component analysis (PCA) of two immune subtypes based on candidate genes. D. Kaplan-Meier analysis showed a difference in overall survival (OS) between two immune subtypes. The *p value* was obtained by the log-rank test. MAD, Median Absolute Deviation.

Figure 3A) between the subtypes for Gene Ontology (GO) analysis in DAVID. GO analysis revealed that genes upregulated in Im2 are enriched in biological processes including

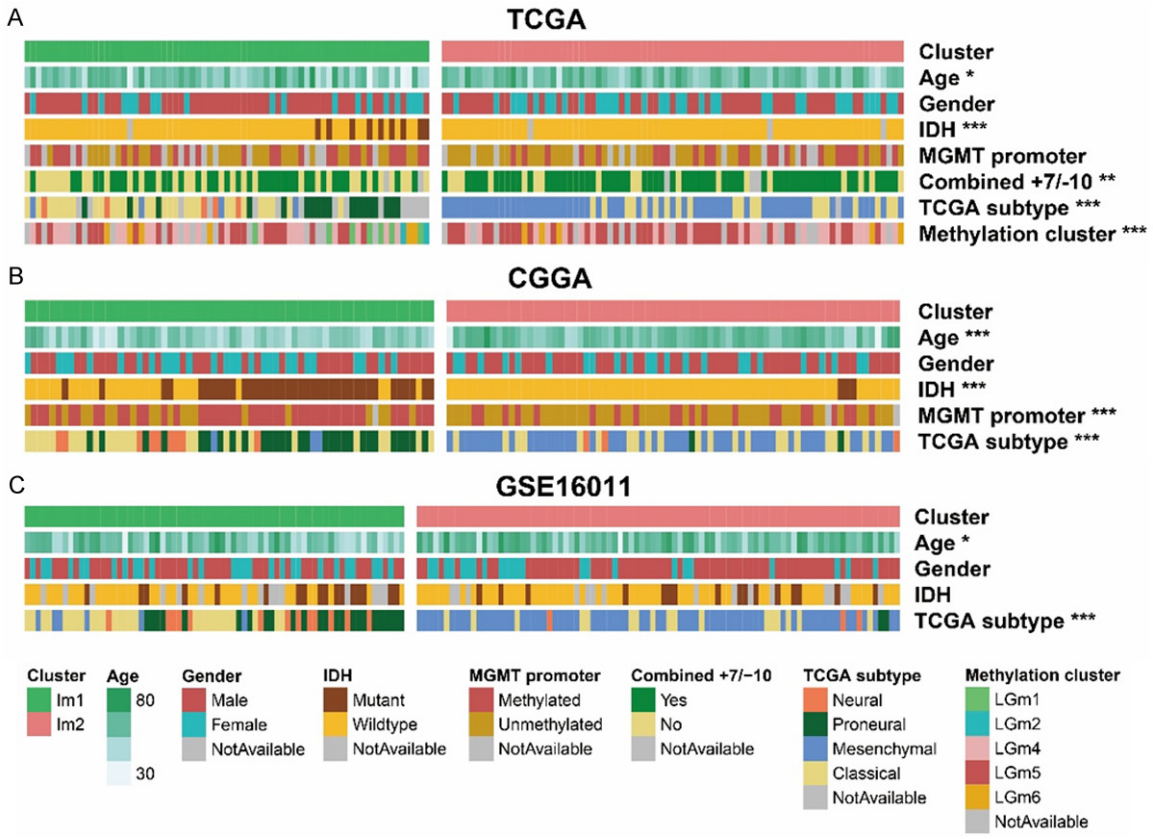

Figure 2. Clinical and molecular differences between two immune subtypes in three datasets. (A) TCGA dataset, (B) CGGA dataset and (C) GSE16011 dataset. IDH, Isocitrate Dehydrogenase; MGMT, O6-Methylguanine-DNA Methyltransferase; Combined +7/-10, Combined Gain Of Entire Chromosome 7 And Loss Of Entire Chromosome 10.

"Immune response", "Inflammatory response", "Chemokine-mediated signaling pathway", "Neutrophil chemotaxis" and "Leukocyte migration" (**Figure 3B**). Whereas the genes downregulated in Im2 were enriched in biological processes of normal neurological function, including "Chemical synaptic transmission", "Regulation of ion transmembrane transport", and "Nervous system development" (Figure S2A). GSEA analysis showed that the pathways enriched in Im2 included "HALLMARK_TNFA_SIGNALING_VIA_NFKB" (NES = 2.67, padj = 6.1e-03), "HALLMARK_INFLAMMATORY_RESPONSE" (NES = 3.01, padj = 6.1e-03), "GO_LEUKOCYTE_ACTIVATION" (NES = 2.48, padj = 6.1e-03), and "GO_IMMUNE_SYSTEM_PROCESS" (NES = 2.41, padj = 6.1e-03) (**Figure 3C**).

Evaluation of immune characteristics of two subtypes

Due to differences in immune enrichment between the two immune subtypes, we further analyzed immune infiltration. First, ESTIMATE analysis [24] revealed that the immune score and stromal score of Im2 were significantly higher than those of Im1, and the tumor purity was significantly lower than that of Im1 ($P < 0.05$, **Figure 3D**). CIBERSORT analysis [25] showed a higher proportion of macrophages in Im2 and a higher proportion of lymphocytes in Im1 ($P < 0.05$, **Figure 3E**). Moreover, HLA and checkpoint gene expression were significantly upregulated in Im2 (**Figure 3F**). To further analyze differences in immunotherapy responses between subtypes, we performed TIDE analysis [28]. We found that Im2 had a significantly lower TIDE score than Im1 ($P = 0.0065$, **Figure 3G**). We also performed the above analysis in the two validation datasets and obtained similar results (Figure S2B-I). Overall, these results indicated that the Im2 subtype in GBM is immune-hot but immune-suppressive, while the Im1 subtype is immune-moderate. Further, patients of Im2 might respond better to immune checkpoint blockade therapy than those of Im1.

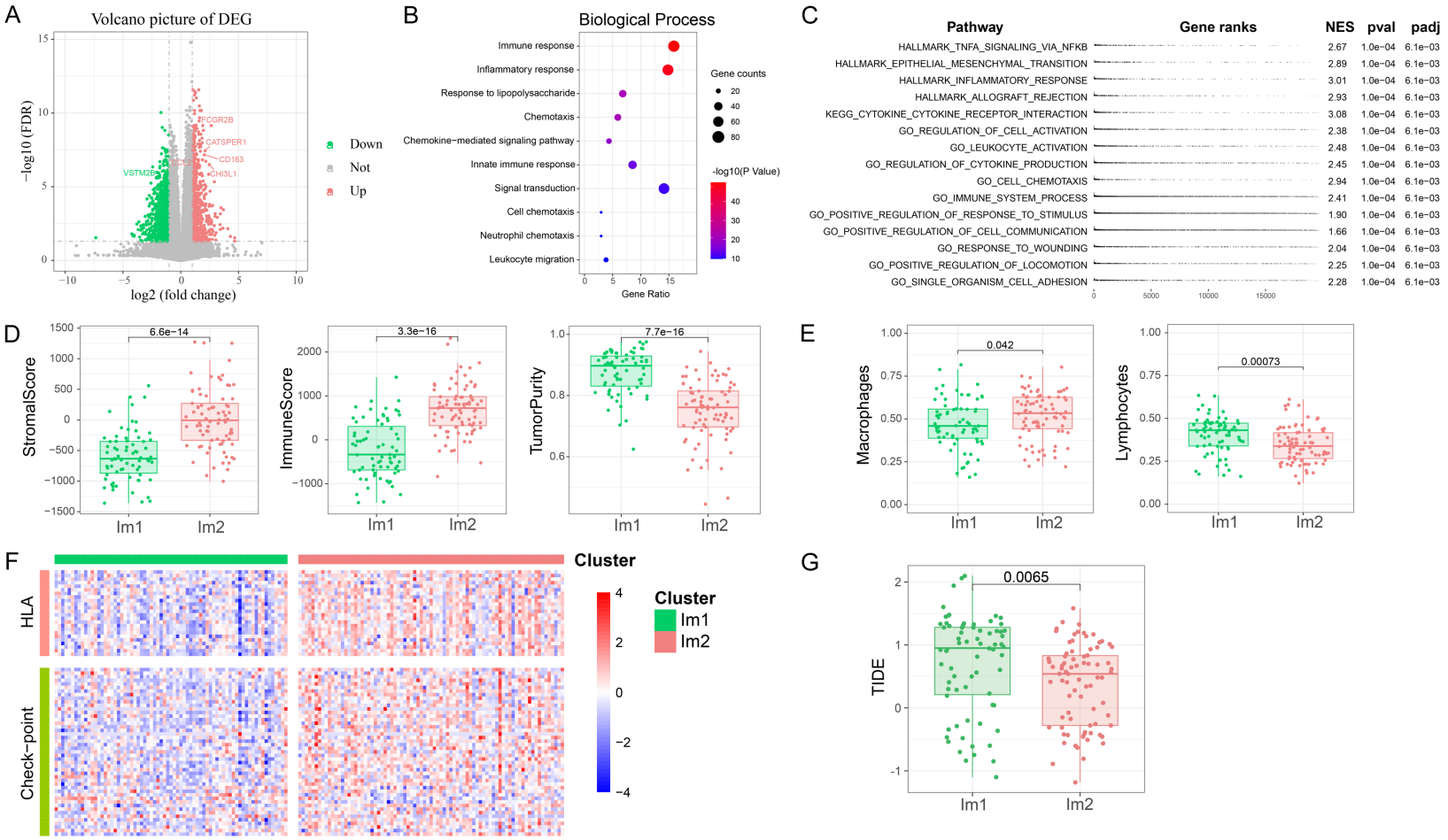

Figure 3. Functional annotation analysis and immune characteristics of two immune subtypes in TCGA dataset. A. The volcano map showed differentially expressed genes between the two immune subtypes. B. Gene Ontology (GO) analysis of up-regulated genes in Im2 subtype. C. Gene set enrichment analysis (GSEA) showed the top 15 pathways enriched in Im2 subtype. D. Stromal score, immune score, and tumor purity from ESTMATE algorithm for two immune subtypes. E. Proportion of macrophages and lymphocytes from CIBERSORT algorithm for two immune subtypes. Macrophages included M0, M1 and M2 macrophages. Lymphocytes included naive B cells, memory B cells, Plasma cells, CD8 T cells, CD4 naive T cells, CD4 memory resting T cells, CD4 memory activated T cells, follicular helper T cells, regulatory T cells (Tregs), gamma delta T cells, resting NK cells, and activated NK cells. F. Heatmap showed HLA and immune checkpoint gene expression levels in two subtypes. G. Boxplot showed TIDE scores in two subtypes.

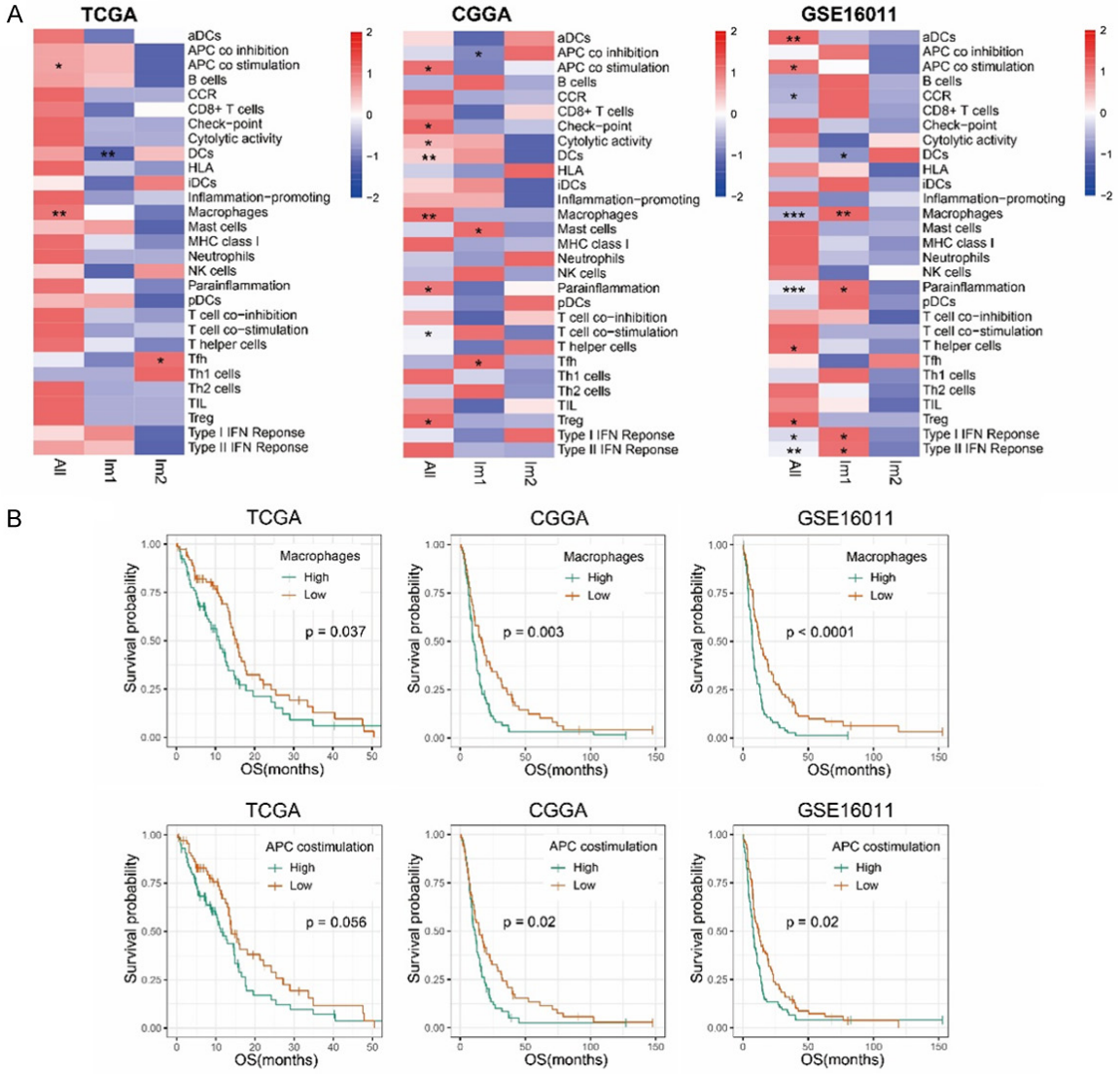

Figure 4. Immune signatures were associated with the prognosis of GBM. A. The heatmaps showed the hazard ratios of 29 immune signatures in Cox regression analysis. *P < 0.05, **P < 0.01, ***P < 0.001. B. Kaplan-Meier analysis of GBM stratified by macrophage and APC co-stimulation scores.

Prognostic analysis of immune response

Considering that tumor immune response can affect the survival of patients [33], we calculated 29 immune signatures [26] for each patient using the ssGSEA method. Among these signatures, APC co-stimulation and macrophages were related to poor outcomes in GBM patients (**Figure 4A** and **4B**). When patients were grouped by subtype, we found that Tfh predicted poor survival in Im2 of the TCGA dataset. Similarly, we selected a group of important immune checkpoint genes to assess their prognostic value. We observed poor prognosis in patients with high expression of TNFRSF14 or TNFSF4 (Figure S3). These results suggested that immune cells or checkpoints in GBM were related to patient prognosis and might serve as potential immunotherapy targets.

Genomic alterations of immune subtypes

To further explore the genomic differences between immune subtypes, we collected somatic mutation and copy-number alterations (CNA) data from the TCGA dataset. In **Figure 5A**, we found that *IDH1* mutations were significantly

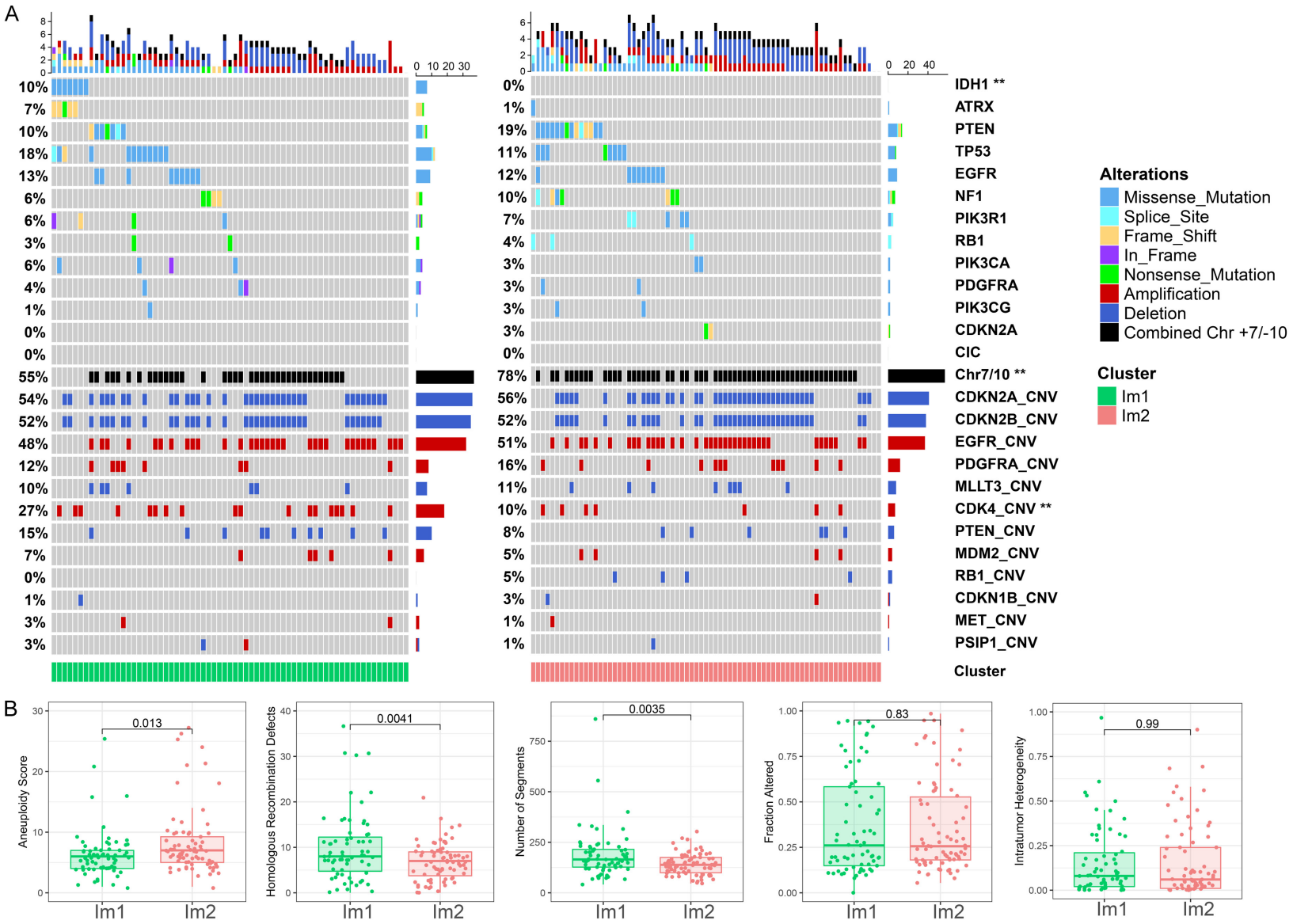

Figure 5. Somatic variation in two immune subtypes of TCGA dataset. A. Somatic mutation and copy-number alterations (CNA) in two immune subtypes. Fisher test, **P < 0.01. B. Measures of DNA damage in two immune subtypes.

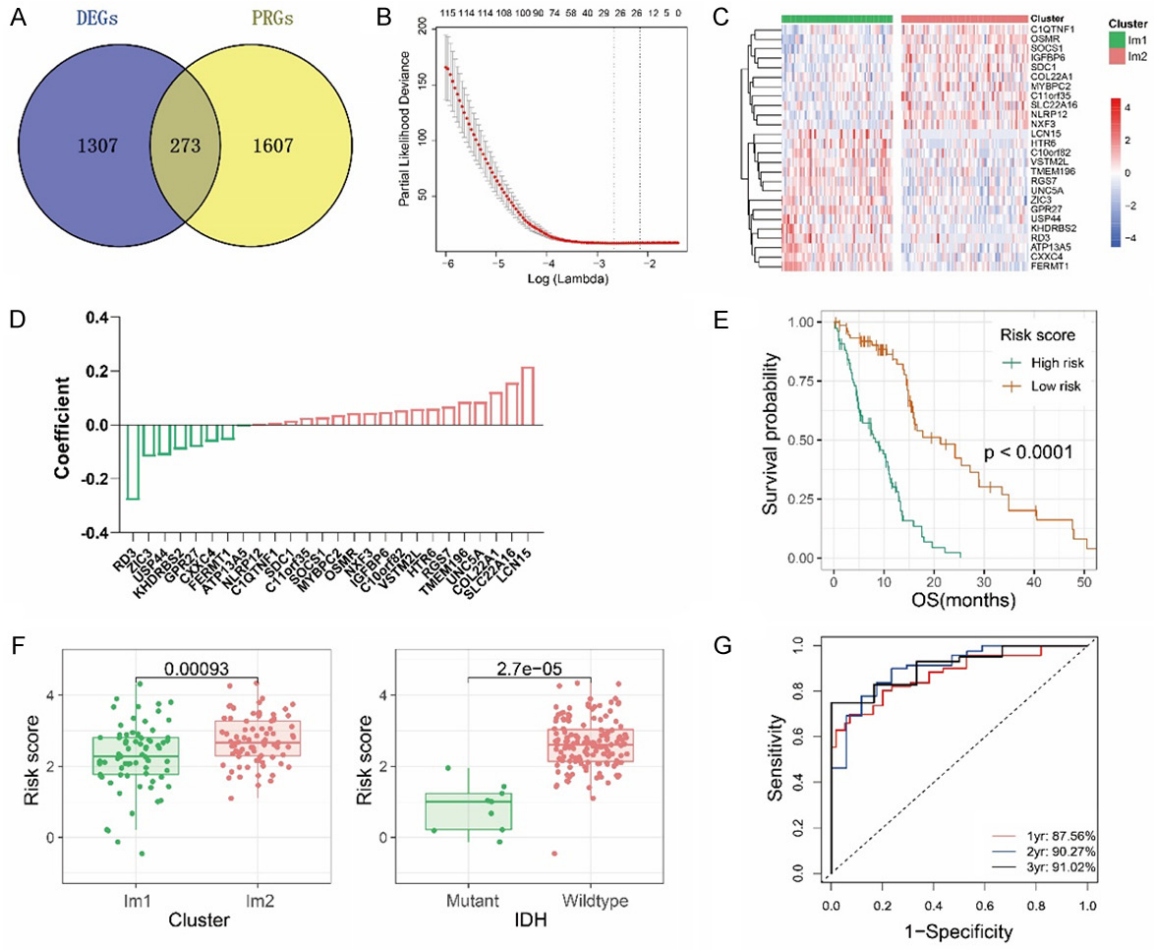

Figure 6. Identification of an immune-related signature in GBM. A. Venn diagram showed differentially expressed genes (DEGs) between two subtypes and prognosis-related genes (PRGs). B. Cross validation for optimizing parameter screening in LASSO regression modeling. C. The heatmap showed the expression of 26 signature genes. D. The regression coefficients of 26 genes in the immune-related signature. E. Kaplan-Meier analysis showed the difference in overall survival (OS) between the high-risk group and the low-risk group. F. Distribution of signature risk score in GBM stratified by immune subtypes and IDH mutation status. G. The timeROC curves showed the 1-year, 2-year, and 3-year AUCs of signature.

enriched in Im1 ($P < 0.05$). The mutation frequency of *ATRX* and *TP53* in Im1 tended to be higher than that in Im2. In Im2, the mutation frequency of *PTEN* tended to be higher than that in Im1, and *CDKN2A* mutation only appeared in Im2. The combined +7/-10 was significantly enriched in Im2. CNA analysis showed that *CDK4* amplification was enriched in Im1, while *RB1* deletion was found only in Im2. In addition, we assessed the measures of DNA damage [19]. Im2 had a significantly higher aneuploidy score than Im1, while Im1 had a significantly higher homologous recombination deficiency and CNV segment burden than Im2 ($P < 0.05$, **Figure 5B**).

Development of an immune-related prognostic signature

Based on our immune classification, we developed an immune-related signature. First, we screened 1580 differentially expressed genes (DEGs, fold change > 2 or < 0.5, FDR < 0.05) between the two subtypes, wherein 273 genes were associated with prognosis in univariate Cox regression analysis (**Figure 6A**, $P < 0.05$, Wald test). We identified 233 genes shared by TCGA and two validation datasets to build an optimal model using the LASSO algorithm (**Figure 6B**). Finally, an immune-related signature of 26 genes (**Figure 6C**) was obtained,

and the score was calculated using regression coefficients (**Figure 6D**). Patients were divided into low-risk and high-risk groups according to the median risk score. The survival curve revealed that the high-risk group lived for a significantly shorter duration than the low-risk group ($P < 0.0001$, **Figure 6E**). The risk scores were significantly higher in the Im2 subtype or IDH-wildtype GBM ($P < 0.05$, **Figure 6F**). Furthermore, the 1-, 2-, and 3-year AUC of the signature was respectively 87.56%, 90.27%, and 91.02% in the ROC curves (**Figure 6G**). In both validation datasets, we calculated the signature score for each patient with regression coefficients of TCGA and obtained similar results (Figure S4). These results confirmed the excellent survival predictive value of our immune-related signature.

Discussion

In view of the significant intra- and inter-tumor heterogeneity of gliomas, numerous glioma classification studies based on different omics data have emerged [31, 32, 34]. Immune profiling has gradually become a feasible method for cancer classification. Thorsson et al. performed immunogenomic analysis of 33 tumor types and classified six immune subtypes [19]. Becht et al. performed immune and stromal classification of colorectal cancer with transcriptome data. The four molecular subtypes showed distinct immune orientations and prognosis [35]. Su et al. evaluated the proportion of immune cells in ccRCC using digital cytometry, and obtained four distinct subtypes by unsupervised clustering [36]. In the present study, we defined two novel subtypes of GBM based on 771 previously reported immune genes. The stability and reproducibility of the two immune subtypes were proved in the validation datasets. There were different clinical, molecular, prognostic, and immune characteristics between the two subtypes, which deepened our understanding of immune heterogeneity in GBM.

We found that patients in Im2 had a significantly worse prognosis. Furthermore, Im2 subtype was closely correlated with *IDH*-wildtype, combined +7/-10, and worse TCGA subtype (mesenchymal). The Im1 subtype was associated with *IDH* mutation and better TCGA subtype (proneural). In the 2021 WHO Classification of CNS Tumors [37], combined +7/-10 has been identified as a biomarker for grade and prognosis, and histologic grade II and III *IDH*-wild type diffuse astrocytoma carrying this molecular feature were designated as *IDH*-wildtype GBM, CNS WHO grade 4. The enrichment of combined +7/-10 in Im2 may be associated with poor prognosis.

Next, we performed functional annotation analysis and found significant differences between the two subtypes in terms of immune and inflammatory responses. We then comprehensively assessed the immune status of the two subtypes, including immune score, proportion of immune cells, and immune checkpoints expression. Im2 showed high immune score and stromal score, low tumor purity, enrichment of macrophages, high expression of immune checkpoint and *HLA* genes, revealing an immune-hot but immune-suppressive tumor microenvironment (TME). Im1 showed low immune and stromal scores, high tumor purity, enrichment of lymphocytes, low expression of immune checkpoint and *HLA* genes, indicating an immune-moderate TME. These findings revealed the immune heterogeneity of GBM. At present, common markers for tumor checkpoint immunotherapy include PD-L1 protein expression, tumor-infiltrating lymphocytes, tumor mutational burden (TMB), microsatellite instability (MSI), and HLA diversity [38, 39]. The TIDE algorithm allowed us to predict patient response to immune checkpoint blockade. We found that Im2 had a significantly lower TIDE score than Im1, revealing the potential immunotherapy predictive value of our classification.

Tumor-associated immune cells show great prospects as prognostic biomarkers. Gentles et al. constructed a prognostic landscape across human cancers to identify tumor-associated leukocytes for prognostic stratification and targeted therapy [33]. Galon et al. analyzed data on tumor-infiltrating immune cells and found that this was a better predictor of prognosis in colorectal cancer patients than current histopathologic methods [40]. Wouters et al. comprehensively reviewed the literature and reported the positive prognostic role of tumor-infiltrating B cells and plasma cells [41]. We evaluated 29 immune signatures through the ssGSEA algorithm and found that macrophage and APC co-stimulation predicted poor prognosis in GBM. Therefore, we speculated

that macrophages enriched in Im2 might be associated with poor prognosis of patients. Then we selected GBM samples (17 of Im1, 5 of Im2) for immunohistochemical analysis, and found that the expression of macrophage-associated markers (IBA1) was significantly upregulated in Im2 (P = 0.032, Figure S5A). Two representative stained sections were showed in Figure S5B and S5C. These clinical samples further confirmed the enrichment of macrophages in Im2.

Similarly, we analyzed 44 common immune checkpoint genes and found a poor prognosis in patients with high expression of TNFRSF14 or TNFSF4 (Figure S3). To further reveal the mechanism of TNFRSF14 or TNFSF4, we first analyzed the expression and found that TNFRSF14 or TNFSF4 was significantly upregulated in IDH-wildtype or Im2 subtype (Figures S6A and S6B, S7A and S7B). Meanwhile, we observed that TNFRSF14 or TNFSF4 was positively correlated with representative immune checkpoint genes, indicating immunosuppressive status in GBM with high expression of TNFRSF14 or TNFSF4 (Figures S6C and S7C). Further, we analyzed the biologic functions of TNFRSF14 or TNFSF4. Genes strongly positively correlated with TNFRSF14 or TNFSF4 (Pearson R > 0.5) were screened and analyzed in Metascape [42]. We found that TNFRSF14 was mainly related to immune and inflammatory responses, and the results of GSEA analysis were consistent (Figure S6D and S6E). Metascape analysis showed that TNFSF4 was mainly associated with malignant biological functions including extracellular matrix organization, angiogenesis and cell-cell adhesion (Figure S7D). GSEA analysis showed that TNFSF4 was also associated with immune and inflammatory responses (Figure S7E). Therefore, it is of great significance to further study the mechanism of TNFRSF14 or TNFSF4 on GBM.

We further explored the genomic differences between immune subtypes and found that *IDH1* mutations were significantly enriched in Im1 which had lower immune scores and macrophages. Consistently, Amankulor et al. reported that *IDH1* mutations lead to downregulation of immune cell infiltration in the glioma microenvironment [43]. Bunse et al. found that *IDH1* mutation-derived R-2-HG impaired activation and proliferation of T cell in gliomas [44]. We also found that the mutation frequency of *ATRX* and *TP53* in Im1 tended to be higher than that in Im2. *ATRX* and *TP53* mutations played key roles in the astrocytic lineage differentiation and development of astrocytoma, and occurred in 80% of Grade II and III astrocytoma. Hu et al. revealed that *ATRX* loss induced T-cell apoptosis and polarization of anti-inflammatory macrophages and infiltration of immunosuppressive regulatory T cells [45]. Additionally, the mutation frequency of *PTEN* in Im2 tended to be higher than that of Im1. Studies have shown that *PTEN*-deficient tumors inhibited the activation of Type I IFN pathway, which in turn impaired the enrichment and activation of antitumor T cells and NK cells [46, 47]. These suggested that somatic alterations might influence immune responses in tumors, and further studies are needed to determine these correlations.

Using differentially expressed genes between the two immune subtypes, we identified an immune-related prognostic signature by LASSO regression modeling. The prognosis was significantly worse in the high-risk group, which appeared more in the Im2 subtype or *IDH*-wildtype GBM. Our signature has shown superior survival predictive potential, but its clinical application value still needs to be evaluated in future investigations.

In summary, we classified GBM from the perspective of immunity and obtained two stable subtypes with different clinical, molecular, prognostic, and immune characteristics. Our study supported the existence of immune heterogeneity in GBM and highlighted the importance of patient stratification in immunotherapy.

Acknowledgements

This work was funded by Provincial Key R&D Program, Science and Technology Department of Zhejiang Province (2017C03018); Key Program of Administration of Traditional Chinese Medicine, Zhejiang Province (2018ZZ015). QWW designed the study and wrote the manuscript. WWL and TJL acquired and integrated data. YJZ and JH conceptualized and supervised the study.

Disclosure of conflict of interest

None.

Address correspondence to: Yongjian Zhu, Department of Neurosurgery, The Second Affiliated Hospital, Zhejiang University School of Medicine. No. 88 Jiefang Road, Hangzhou 310009, Zhejiang, China. Tel: +86-571-87784715; Fax: +86-571-87784715; E-mail: neurosurgery@zju.edu.cn; Jue Hu, School of Basic Medical Sciences and Forensic Medicine, Hangzhou Medical College, No. 8 Yikang Road, Hangzhou 311399, Zhejiang, China. Tel: +86-571-87692630; Fax: +86-571-87692630; E-mail: hj@hmc.edu.cn

References

[1] Jiang T, Nam DH, Ram Z, Poon WS, Wang J, Boldbaatar D, Mao Y, Ma W, Mao Q, You Y, Jiang C, Yang X, Kang C, Qiu X, Li W, Li S, Chen L, Li X, Liu Z, Wang W, Bai H, Yao Y, Li S, Wu A, Sai K, Li G, Yao K, Wei X, Liu X, Zhang Z, Dai Y, Lv S, Wang L, Lin Z, Dong J, Xu G, Ma X, Zhang W, Zhang C, Chen B, You G, Wang Y, Wang Y, Bao Z, Yang P, Fan X, Liu X, Zhao Z, Wang Z, Li Y, Wang Z, Li G, Fang S, Li L, Liu Y, Liu S, Shan X, Liu Y, Chai R, Hu H, Chen J, Yan W, Cai J, Wang H, Chen L, Yang Y, Wang Y, Han L and Wang Q. Clinical practice guidelines for the management of adult diffuse gliomas. Cancer Lett 2021; 499: 60-72.

[2] Ostrom QT, Gittleman H, Truitt G, Boscia A, Kruchko C and Barnholtz-Sloan JS. CBTRUS statistical report: primary brain and other central nervous system tumors diagnosed in the United States in 2011-2015. Neuro Oncol 2018; 20 Suppl 4: iv1-iv86.

[3] Tan AC, Ashley DM, López GY, Malinzak M, Friedman HS and Khasraw M. Management of glioblastoma: state of the art and future directions. CA Cancer J Clin 2020; 70: 299-312.

[4] Stupp R, Hegi ME, Mason WP, van den Bent MJ, Taphoorn MJ, Janzer RC, Ludwin SK, Allgeier A, Fisher B, Belanger K, Hau P, Brandes AA, Gijtenbeek J, Marosi C, Vecht CJ, Mokhtari K, Wesseling P, Villa S, Eisenhauer E, Gorlia T, Weller M, Lacombe D, Cairncross JG and Mirimanoff RO. Effects of radiotherapy with concomitant and adjuvant temozolomide versus radiotherapy alone on survival in glioblastoma in a randomised phase III study: 5-year analysis of the EORTC-NCIC trial. Lancet Oncol 2009; 10: 459-466.

[5] Wang QW, Sun LH, Zhang Y, Wang Z, Zhao Z, Wang ZL, Wang KY, Li GZ, Xu JB, Ren CY, Ma WP, Wang HJ, Li SW, Zhu YJ, Jiang T and Bao ZS. MET overexpression contributes to STAT4-PD-L1 signaling activation associated with tumor-associated, macrophages-mediated immunosuppression in primary glioblastomas. J Immunother Cancer 2021; 9: e002451.

[6] Lim M, Xia Y, Bettegowda C and Weller M. Current state of immunotherapy for glioblastoma. Nat Rev Clin Oncol 2018; 15: 422-442.

[7] Sampson JH, Gunn MD, Fecci PE and Ashley DM. Brain immunology and immunotherapy in brain tumours. Nat Rev Cancer 2020; 20: 12-25.

[8] Weller M, Butowski N, Tran DD, Recht LD, Lim M, Hirte H, Ashby L, Mechtler L, Goldlust SA, Iwamoto F, Drappatz J, O'Rourke DM, Wong M, Hamilton MG, Finocchiaro G, Perry J, Wick W, Green J, He Y, Turner CD, Yellin MJ, Keler T, Davis TA, Stupp R and Sampson JH. Rindopepimut with temozolomide for patients with newly diagnosed, EGFRvIII-expressing glioblastoma (ACT IV): a randomised, double-blind, international phase 3 trial. Lancet Oncol 2017; 18: 1373-1385.

[9] Wen PY, Reardon DA, Armstrong TS, Phuphanich S, Aiken RD, Landolfi JC, Curry WT, Zhu JJ, Glantz M, Peereboom DM, Markert JM, LaRocca R, O'Rourke DM, Fink K, Kim L, Gruber M, Lesser GJ, Pan E, Kesari S, Muzikansky A, Pinilla C, Santos RG and Yu JS. A randomized double-blind placebo-controlled phase II trial of dendritic cell vaccine ICT-107 in newly diagnosed patients with glioblastoma. Clin Cancer Res 2019; 25: 5799-5807.

[10] O'Rourke DM, Nasrallah MP, Desai A, Melenhorst JJ, Mansfield K, Morrissette JJD, Martinez-Lage M, Brem S, Maloney E, Shen A, Isaacs R, Mohan S, Plesa G, Lacey SF, Navenot JM, Zheng Z, Levine BL, Okada H, June CH, Brogdon JL and Maus MV. A single dose of peripherally infused EGFRvIII-directed CAR T cells mediates antigen loss and induces adaptive resistance in patients with recurrent glioblastoma. Sci Transl Med 2017; 9: eaaa0984.

[11] Reardon DA, Gokhale PC, Klein SR, Ligon KL, Rodig SJ, Ramkissoon SH, Jones KL, Conway AS, Liao XY, Zhou J, Wen PY, Van Den Abbeele AD, Hodi FS, Qin L, Kohl NE, Sharpe AH, Dranoff G and Freeman GJ. Glioblastoma eradication following immune checkpoint blockade in an orthotopic, immunocompetent model. Cancer Immunol Res 2016; 4: 124-135.

[12] Zeng J, See AP, Phallen J, Jackson CM, Belcaid Z, Ruzevick J, Durham N, Meyer C, Harris TJ, Albesiano E, Pradilla G, Ford E, Wong J, Hammers HJ, Mathios D, Tyler B, Brem H, Tran PT, Pardoll D, Drake CG and Lim M. Anti-PD-1 blockade and stereotactic radiation produce long-term survival in mice with intracranial gliomas. Int J Radiat Oncol Biol Phys 2013; 86: 343-349.

[13] Reardon DA, Brandes AA, Omuro A, Mulholland P, Lim M, Wick A, Baehring J, Ahluwalia MS, Roth P, Bahr O, Phuphanich S, Sepulveda JM, De Souza P, Sahebjam S, Carleton M, Tatsuoka

K, Taitt C, Zwirtes R, Sampson J and Weller M. Effect of nivolumab vs bevacizumab in patients with recurrent glioblastoma the checkmate 143 phase 3 randomized clinical trial. JAMA Oncol 2020; 6: 1003-1010.

[14] Sampson JH, Omuro AMP, Preusser M, Lim M, Butowski NA, Cloughesy TF, Strauss LC, Latek RR, Paliwal P, Weller M and Reardon DA. A randomized, phase 3, open-label study of nivolumab versus temozolomide (TMZ) in combination with radiotherapy (RT) in adult patients (pts) with newly diagnosed, O-6-methylguanine DNA methyltransferase (MGMT)-unmethylated glioblastoma (GBM): CheckMate-498. J Clin Oncol 2016; 34: 2.

[15] Bristol Myers Squibb announces update on phase 3 CheckMate-548 trial evaluating patients with newly diagnosed MGMT-methylated glioblastoma multiforme. Bristol Myers Squibb 2020.

[16] Lichty BD, Breitbach CJ, Stojdl DF and Bell JC. Going viral with cancer immunotherapy. Nat Rev Cancer 2014; 14: 559-567.

[17] Liu P, Wang Y, Wang Y, Kong Z, Chen W, Li J, Chen W, Tong Y, Ma W and Wang Y. Effects of oncolytic viruses and viral vectors on immunity in glioblastoma. Gene Ther 2022; 29: 115-126.

[18] Jackson CM, Choi J and Lim M. Mechanisms of immunotherapy resistance: lessons from glioblastoma. Nat Immunol 2019; 20: 1100-1109.

[19] Thorsson V, Gibbs DL, Brown SD, Wolf D, Bortone DS, Ou Yang TH, Porta-Pardo E, Gao GF, Plaisier CL, Eddy JA, Ziv E, Culhane AC, Paull EO, Sivakumar IKA, Gentles AJ, Malhotra R, Farshidfar F, Colaprico A, Parker JS, Mose LE, Vo NS, Liu J, Liu Y, Rader J, Dhankani V, Reynolds SM, Bowlby R, Califano A, Cherniack AD, Anastassiou D, Bedognetti D, Mokrab Y, Newman AM, Rao A, Chen K, Krasnitz A, Hu H, Malta TM, Noushmehr H, Pedamallu CS, Bullman S, Ojesina AI, Lamb A, Zhou W, Shen H, Choueiri TK, Weinstein JN, Guinney J, Saltz J, Holt RA, Rabkin CS; Cancer Genome Atlas Research Network, Lazar AJ, Serody JS, Demicco EG, Disis ML, Vincent BG and Shmulevich I. The immune landscape of cancer. Immunity 2018; 48: 812-830, e14.

[20] Zhao Z, Zhang KN, Wang QW, Li GZ, Zeng F, Zhang Y, Wu F, Chai RC, Wang Z, Zhang CB, Zhang W, Bao ZS and Jiang T. Chinese glioma genome atlas (CGGA): a comprehensive resource with functional genomic data from chinese glioma patients. Genomics Proteomics Bioinformatics 2021; 19: 1-12.

[21] Gravendeel LA, Kouwenhoven MC, Gevaert O, de Rooi JJ, Stubbs AP, Duijm JE, Daemen A, Bleeker FE, Bralten LB, Kloosterhof NK, De Moor B, Eilers PH, van der Spek PJ, Kros JM, Sillevis Smitt PA, van den Bent MJ and French PJ. Intrinsic gene expression profiles of gliomas are a better predictor of survival than histology. Cancer Res 2009; 69: 9065-9072.

[22] Wang QW, Bao ZS, Jiang T and Zhu YJ. Tumor microenvironment is associated with clinical and genetic properties of diffuse gliomas and predicts overall survival. Cancer Immunol Immunother 2022; 71: 953-966.

[23] Charoentong P, Finotello F, Angelova M, Mayer C, Efremova M, Rieder D, Hackl H and Trajanoski Z. Pan-cancer immunogenomic analyses reveal genotype-immunophenotype relationships and predictors of response to checkpoint blockade. Cell Rep 2017; 18: 248-262.

[24] Yoshihara K, Shahmoradgoli M, Martinez E, Vegesna R, Kim H, Torres-Garcia W, Trevino V, Shen H, Laird PW, Levine DA, Carter SL, Getz G, Stemke-Hale K, Mills GB and Verhaak RG. Inferring tumour purity and stromal and immune cell admixture from expression data. Nat Commun 2013; 4: 11.

[25] Newman AM, Liu CL, Green MR, Gentles AJ, Feng WG, Xu Y, Hoang CD, Diehn M and Alizadeh AA. Robust enumeration of cell subsets from tissue expression profiles. Nat Methods 2015; 12: 453-7.

[26] He Y, Jiang ZH, Chen C and Wang XS. Classification of triple-negative breast cancers based on immunogenomic profiling. J Exp Clin Cancer Res 2018; 37: 327.

[27] Huang da W, Sherman BT and Lempicki RA. Systematic and integrative analysis of large gene lists using DAVID bioinformatics resources. Nat Protoc 2009; 4: 44-57.

[28] Fu JX, Li KR, Zhang WB, Wan CX, Zhang J, Jiang P and Liu XS. Large-scale public data reuse to model immunotherapy response and resistance. Genome Med 2020; 12: 21.

[29] Wang QW, Wang ZL, Li GZ, Zhang CB, Bao ZS, Wang Z, You G and Jiang T. Identification of IDH-mutant gliomas by a prognostic signature according to gene expression profiling. Aging (Albany NY) 2018; 10: 1977-1988.

[30] Tibshirani R, Hastie T, Narasimhan B and Chu G. Diagnosis of multiple cancer types by shrunken centroids of gene expression. Proc Natl Acad Sci U S A 2002; 99: 6567-6572.

[31] Brennan CW, Verhaak RG, McKenna A, Campos B, Noushmehr H, Salama SR, Zheng S, Chakravarty D, Sanborn JZ, Berman SH, Beroukhim R, Bernard B, Wu CJ, Genovese G, Shmulevich I, Barnholtz-Sloan J, Zou L, Vegesna R, Shukla SA, Ciriello G, Yung WK, Zhang W, Sougnez C, Mikkelsen T, Aldape K, Bigner DD, Van Meir EG, Prados M, Sloan A, Black KL, Eschbacher J, Finocchiaro G, Friedman W, Andrews DW, Guha A, Iacocca M, O'Neill BP, Foltz

G, Myers J, Weisenberger DJ, Penny R, Kucherlapati R, Perou CM, Hayes DN, Gibbs R, Marra M, Mills GB, Lander E, Spellman P, Wilson R, Sander C, Weinstein J, Meyerson M, Gabriel S, Laird PW, Haussler D, Getz G and Chin L; TCGA Research Network. The somatic genomic landscape of glioblastoma. Cell 2013; 155: 462-477.

[32] Ceccarelli M, Barthel FP, Malta TM, Sabedot TS, Salama SR, Murray BA, Morozova O, Newton Y, Radenbaugh A, Pagnotta SM, Anjum S, Wang J, Manyam G, Zoppoli P, Ling S, Rao AA, Grifford M, Cherniack AD, Zhang H, Poisson L, Carlotti CG Jr, Tirapelli DP, Rao A, Mikkelsen T, Lau CC, Yung WK, Rabadan R, Huse J, Brat DJ, Lehman NL, Barnholtz-Sloan JS, Zheng S, Hess K, Rao G, Meyerson M, Beroukhim R, Cooper L, Akbani R, Wrensch M, Haussler D, Aldape KD, Laird PW, Gutmann DH; TCGA Research Network, Noushmehr H, Iavarone A and Verhaak RG. Molecular profiling reveals biologically discrete subsets and pathways of progression in diffuse glioma. Cell 2016; 164: 550-563.

[33] Gentles AJ, Newman AM, Liu CL, Bratman SV, Feng WG, Kim D, Nair VS, Xu Y, Khuong A, Hoang CD, Diehn M, West RB, Plevritis SK and Alizadeh AA. The prognostic landscape of genes and infiltrating immune cells across human cancers. Nat Med 2015; 21: 938-945.

[34] Wenger A, Vega SF, Kling T, Bontell TO, Jakola AS and Caren H. Intratumor DNA methylation heterogeneity in glioblastoma: implications for DNA methylation-based classification. Neuro Oncol 2019; 21: 616-627.

[35] Becht E, de Reynies A, Giraldo NA, Pilati C, Buttard B, Lacroix L, Selves J, Sautes-Fridman C, Laurent-Puig P and Fridman WH. Immune and stromal classification of colorectal cancer is associated with molecular subtypes and relevant for precision immunotherapy. Clin Cancer Res 2016; 22: 4057-4066.

[36] Su S, Akbarinejad S and Shahriyari L. Immune classification of clear cell renal cell carcinoma. Sci Rep 2021; 11: 4338.

[37] Louis DN, Perry A, Wesseling P, Brat DJ, Cree IA, Figarella-Branger D, Hawkins C, Ng HK, Pfister SM, Reifenberger G, Soffietti R, von Deimling A and Ellison DW. The 2021 WHO classification of tumors of the central nervous system: a summary. Neuro Oncol 2021; 23: 1231-1251.

[38] Gibney GT, Weiner LM and Atkins MB. Predictive biomarkers for checkpoint inhibitor-based immunotherapy. Lancet Oncol 2016; 17: E542-E551.

[39] Cristescu R, Mogg R, Ayers M, Albright A, Murphy E, Yearley J, Sher X, Liu XQ, Lu H, Nebozhyn M, Zhang C, Lunceford JK, Joe A, Cheng J, Webber AL, Ibrahim N, Plimack ER, Ott PA, Seiwert TY, Ribas A, McClanahan TK, Tomassini JE, Loboda A and Kaufman D. Pan-tumor genomic biomarkers for PD-1 checkpoint blockade-based immunotherapy. Science 2018; 362: eaar3593.

[40] Galon J, Costes A, Sanchez-Cabo F, Kirilovsky A, Mlecnik B, Lagorce-Pages C, Tosolini M, Camus M, Berger A, Wind P, Zinzindohoue F, Bruneval P, Cugnenc PH, Trajanoski Z, Fridman WH and Pagès F. Type, density, and location of immune cells within human colorectal tumors predict clinical outcome. Science 2006; 313: 1960-1964.

[41] Wouters MCA and Nelson BH. Prognostic significance of tumor-infiltrating B cells and plasma cells in human cancer. Clin Cancer Res 2018; 24: 6125-6135.

[42] Zhou Y, Zhou B, Pache L, Chang M, Khodabakhshi AH, Tanaseichuk O, Benner C and Chanda SK. Metascape provides a biologist-oriented resource for the analysis of systems-level datasets. Nat Commun 2019; 10: 1523.

[43] Amankulor NM, Kim Y, Arora S, Kargl J, Szulzewsky F, Hanke M, Margineantu DH, Rao A, Bolouri H, Delrow J, Hockenbery D, Houghton AM and Holland EC. Mutant IDH1 regulates the tumor-associated immune system in gliomas. Genes Dev 2017; 31: 774-786.

[44] Bunse L, Pusch S, Bunse T, Sahm F, Sanghvi K, Friedrich M, Alansary D, Sonner JK, Green E, Deumelandt K, Kilian M, Neftel C, Uhlig S, Kessler T, von Landenberg A, Berghoff AS, Marsh K, Steadman M, Zhu D, Nicolay B, Wiestler B, Breckwoldt MO, Al-Ali R, Karcher-Bausch S, Bozza M, Oezen I, Kramer M, Meyer J, Habel A, Eisel J, Poschet G, Weller M, Preusser M, Nadji-Ohl M, Thon N, Burger MC, Harter PN, Ratliff M, Harbottle R, Benner A, Schrimpf D, Okun J, Herold-Mende C, Turcan S, Kaulfuss S, Hess-Stumpp H, Bieback K, Cahill DP, Plate KH, Hänggi D, Dorsch M, Suvà ML, Niemeyer BA, von Deimling A, Wick W and Platten M. Suppression of antitumor T cell immunity by the oncometabolite (R)-2-hydroxyglutarate. Nat Med 2018; 24: 1192-1203.

[45] Hu C, Wang K, Damon C, Fu Y, Ma T, Kratz L, Lal B, Ying M, Xia S, Cahill DP, Jackson CM, Lim M, Laterra J and Li Y. ATRX loss promotes immunosuppressive mechanisms in IDH1 mutant glioma. Neuro Oncol 2022; 24: 888-900.

[46] Vidotto T, Melo CM, Castelli E, Koti M, Dos Reis RB and Squire JA. Emerging role of PTEN loss in evasion of the immune response to tumours. Br J Cancer 2020; 122: 1732-1743.

[47] Fuertes MB, Woo SR, Burnett B, Fu YX and Gajewski TF. Type I interferon response and innate immune sensing of cancer. Trends Immunol 2013; 34: 67-73.

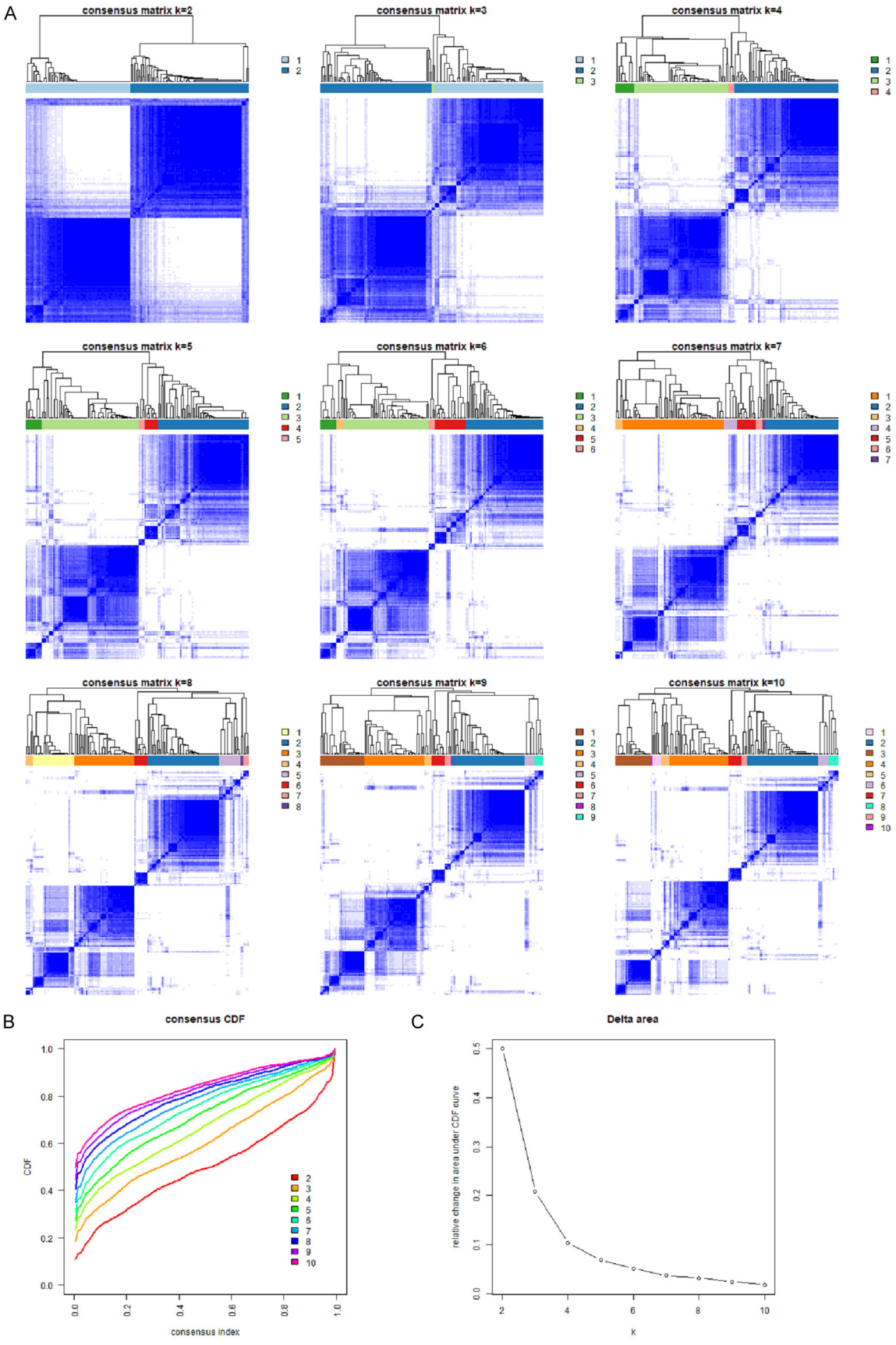
A
consensus matrix k=2
consensus matrix k=3
consensus matrix k=4
consensus matrix k=5
consensus matrix k=6
consensus matrix k=7
consensus matrix k=8
consensus matrix k=9
consensus matrix k=10
B
consensus CDF
CDF
consensus index
C
Delta area
relative change in area under CDF curve
k

Figure S1. Consensus clustering based on immune gene expression of GBM from TCGA dataset. A. Clustering matrix for k=2 to k=10. B. CDF (cumulative distribution function) curve for k=2 to k=10. C. Relative change in area under CDF curve for k=2 to k=10.

Table S1. IGP was estimated for each immune subtype in the validation datasets

Immune subtype	CGGA	GSE16011
Im1	0.917	0.873
Im2	0.806	0.900

Table S2. Clinical characteristics of patients with distinct immune subtypes in TCGA dataset

Variable	Im1 n=71	Im2 n=81	*P* value
Age			0.046*
≤ 45 years	14	6	
> 45 years	57	75	
Gender			0.052
Female	19	35	
Male	52	46	
IDH			< 0.001*
Mutant	9	0	
Wildtype	61	78	
NA	1	3	
MGMT promoter			0.334
Methylated	27	25	
Unmethylated	29	41	
NA	15	15	
Combined chromosome +7/-10			0.005*
Yes	37	60	
No	32	18	
NA	2	3	
TCGA transcriptome subtype			< 0.001*
Mesenchymal	4	60	
Classical	29	20	
Neural	5	0	
Proneural	18	0	
NA	15	1	
Methylation cluster			< 0.001*
LGm1	7	0	
LGm2	2	0	
LGm3	0	0	
LGm4	20	23	
LGm5	21	38	
LGm6	6	5	
NA	15	15	

*P < 0.05.

Table S3. Clinical characteristics of patients with distinct immune subtypes in CGGA dataset

Variable	Im1 n=66	Im2 n=73	*P* value
Age			< 0.001*
≤ 45 years	43	18	
> 45 years	23	55	
Gender			0.247
Female	28	23	
Male	38	50	
IDH			< 0.001*
Mutant	38	3	
Wildtype	28	70	
MGMT promoter			< 0.001*
Methylated	45	21	
Unmethylated	20	50	
NA	1	2	
TCGA transcriptome subtype			< 0.001*
Mesenchymal	3	46	
Classical	25	22	
Neural	9	3	
Proneural	29	2	

*P < 0.05.

Table S4. Clinical characteristics of patients with distinct immune subtypes in GSE16011 dataset

Variable	Im1 n=70	Im2 n=89	*P* value
Age			0.031*
≤ 45 years	23	15	
> 45 years	47	74	
Gender			0.084
Female	28	23	
Male	42	66	
IDH			0.344
Mutant	17	16	
Wildtype	38	57	
NA	15	16	
TCGA transcriptome subtype			< 0.001*
Mesenchymal	6	67	
Classical	27	17	
Neural	13	3	
Proneural	24	2	

*P < 0.05.

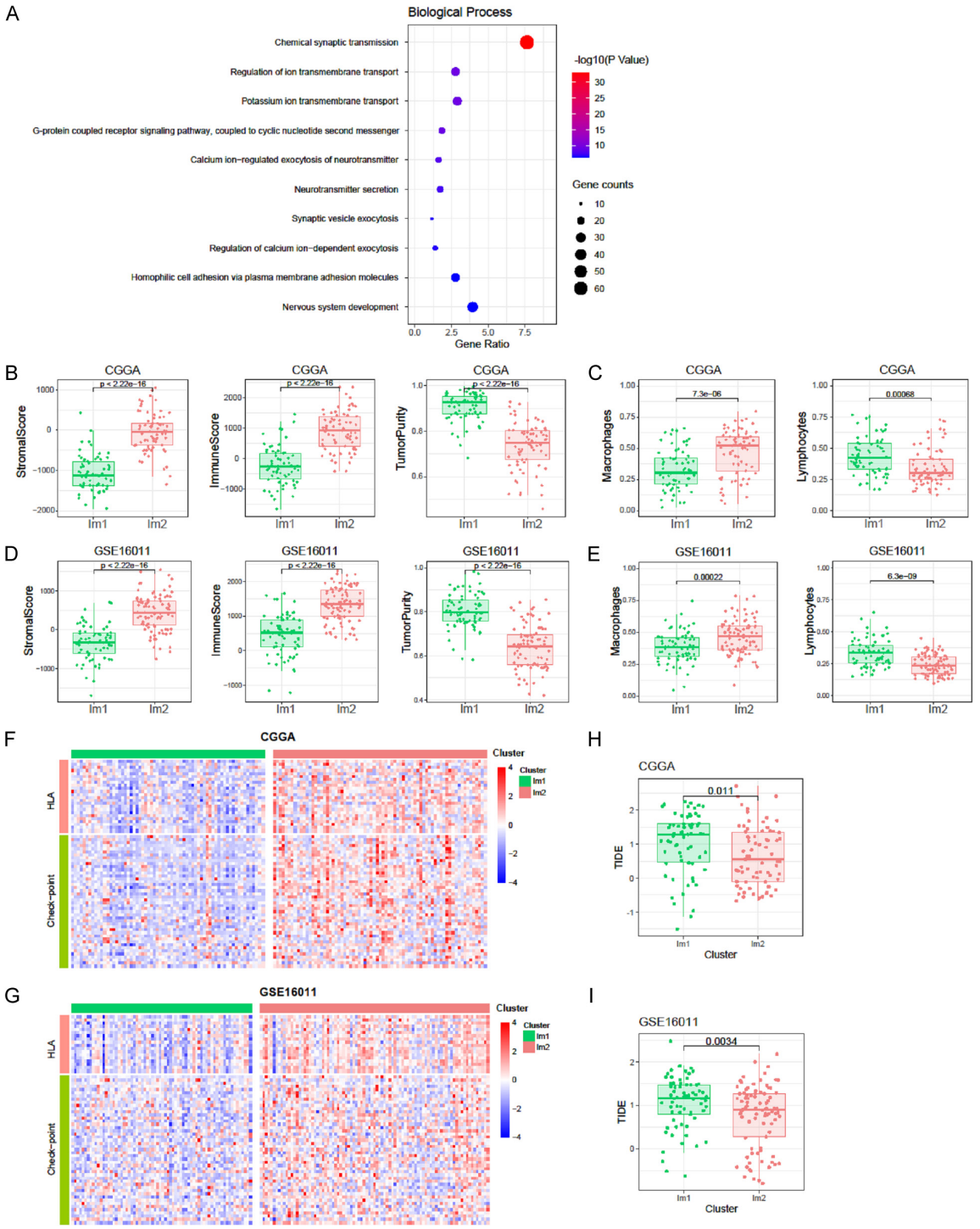

Figure S2. Functional annotation analysis and immune characteristics of two immune subtypes. (A) Gene Ontology (GO) analysis of down-regulated genes in Im2 subtype of TCGA dataset. Stromal score, immune score, and tumor purity from ESTMATE algorithm for two immune subtypes in CGGA (B) and GSE16011 (D) datasets. Proportion of macrophages and lymphocytes from CIBERSORT algorithm for two immune subtypes in CGGA (C) and GSE16011 (E) datasets. Heatmap showed HLA and immune checkpoint gene expression levels for two immune subtypes in CGGA (F) and GSE16011 (G) datasets. Boxplot showed TIDE scores for two immune subtypes in CGGA (H) and GSE16011 (I) datasets.

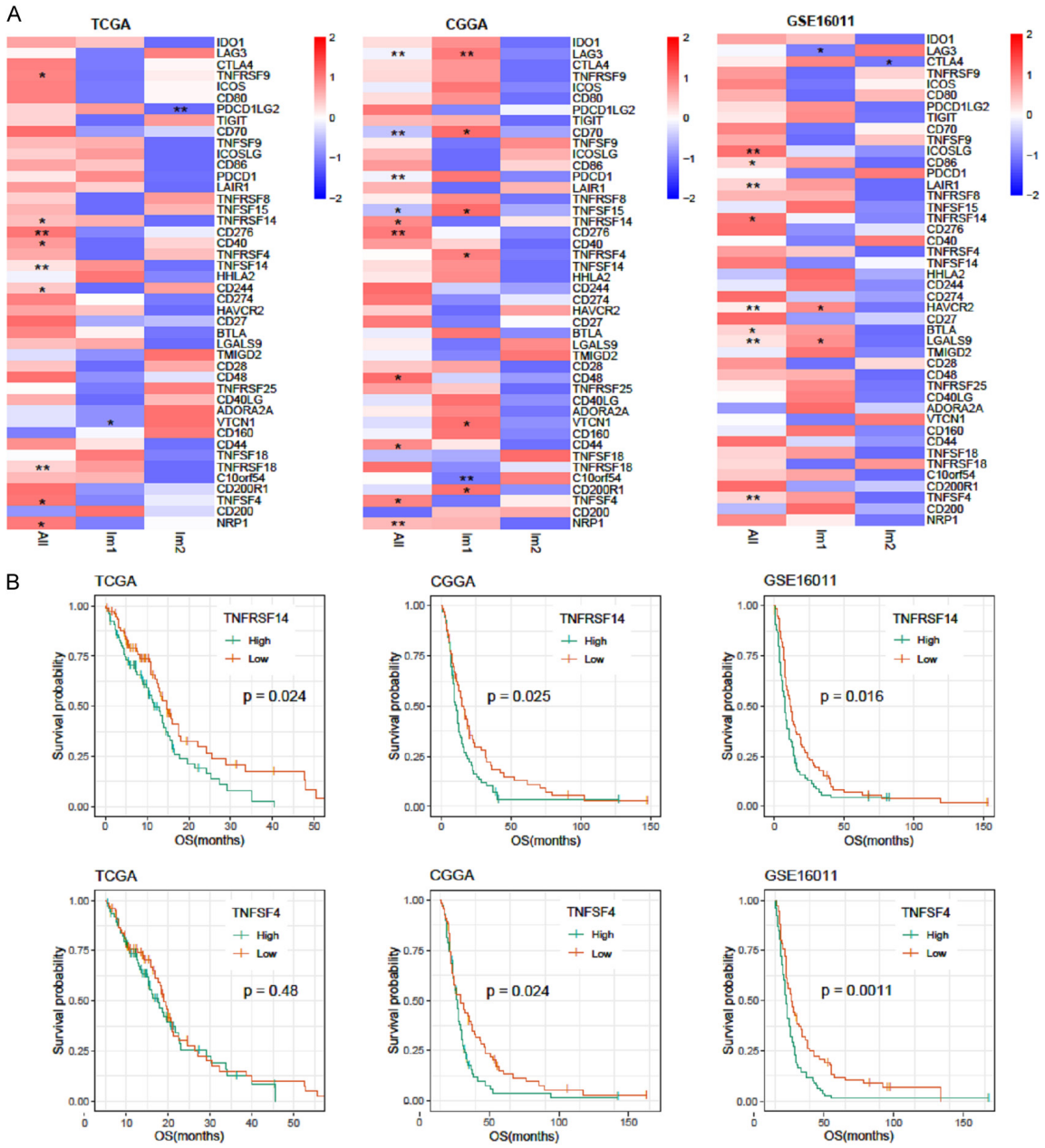

Figure S3. Immune checkpoint genes were associated with the prognosis of GBM. A. The heatmaps showed the hazard ratios of immune checkpoint gene expression in Cox regression analysis. *P < 0.05, **P < 0.01, ***P < 0.001. B. Kaplan-Meier analysis of GBM stratified by expression of TNFRSF14 and TNFSF4.

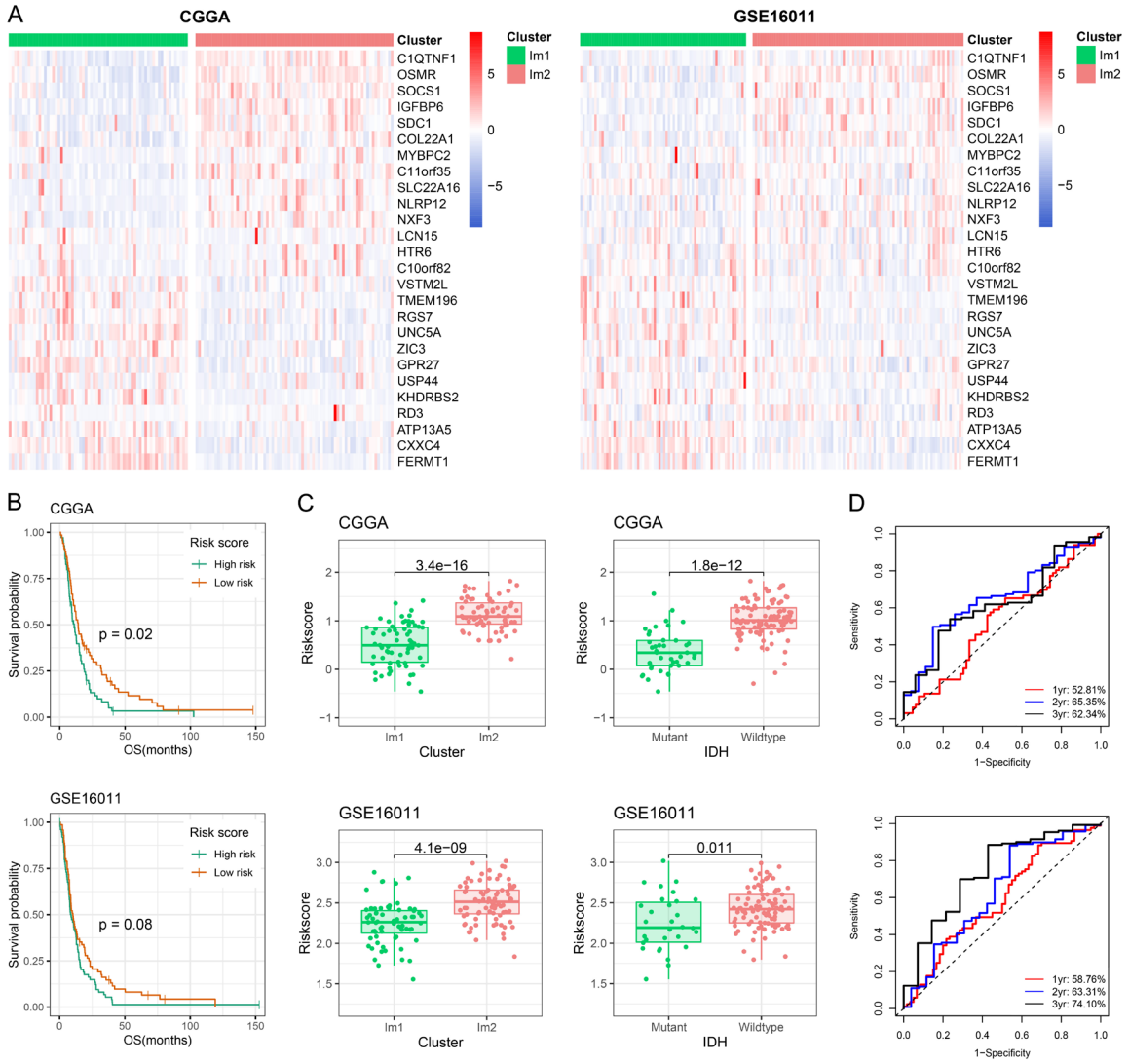

Figure S4. Validation of the obtained immune-related signature in CGGA and GSE16011 datasets. A. Heatmaps show the signature gene expression in CGGA and GSE16011 datasets. B. Kaplan-Meier analysis of the immune-related signature in GBM. *P* value was calculated by the log-rank test. C. Distribution of signature risk score in GBM stratified by immune subtypes and IDH mutation status. D. The timeROC curves showed the 1-year, 2-year and 3-year AUC of signature.

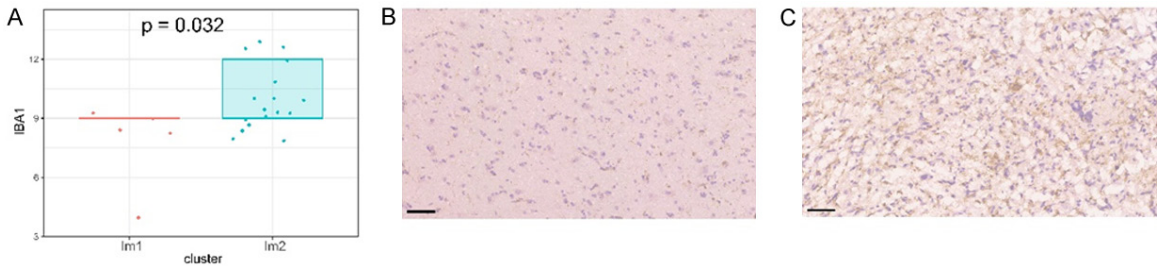

Figure S5. The IBA1 protein expression in Im1 and Im2 (A). Representative photographs of immunohistochemical staining of IBA1 in Im1 (B) and Im2 (C). Positive cells are stained brown. Scale bar, 60 μm.

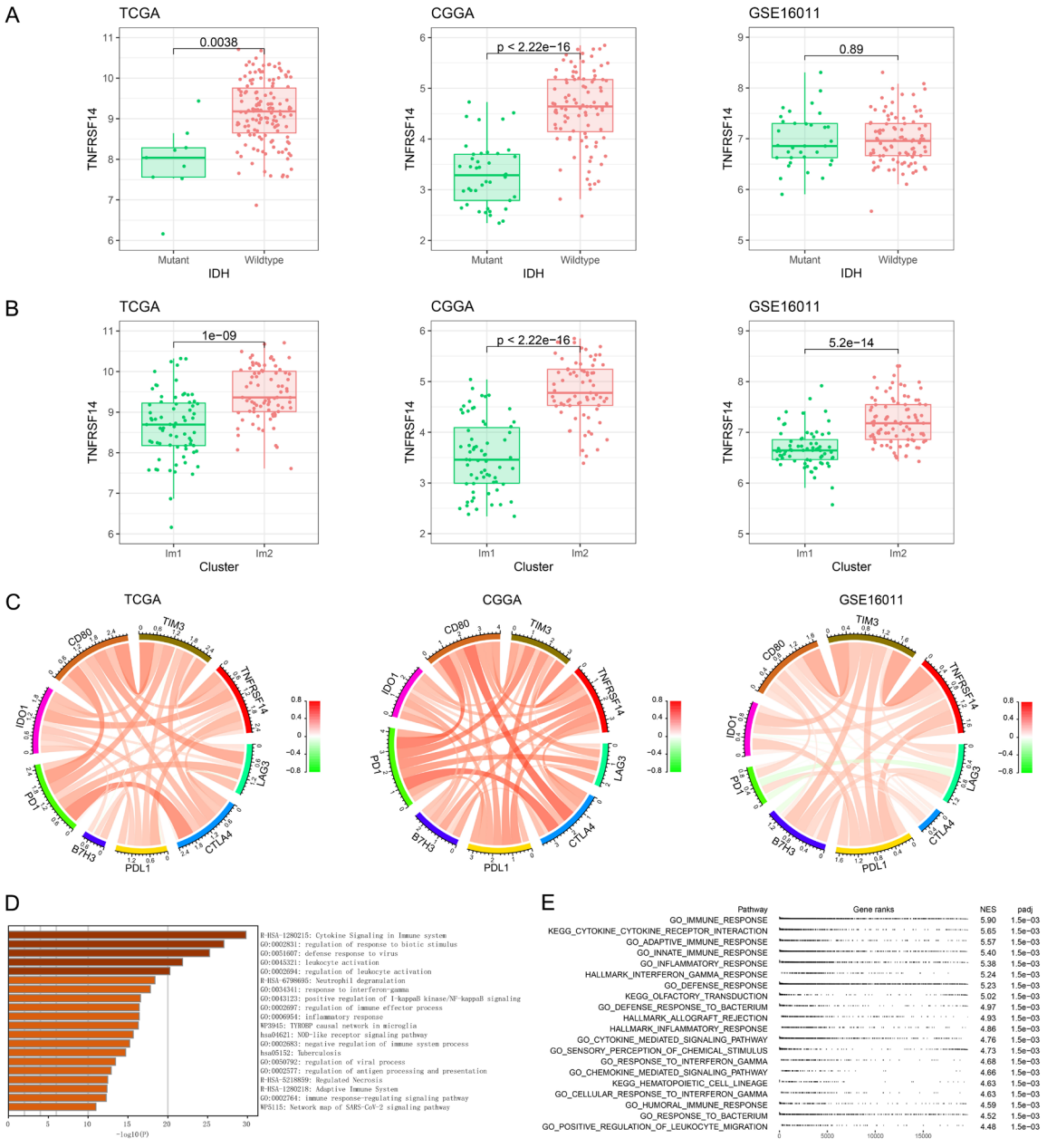

Figure S6. TNFRSF14 expression in three datasets according to IDH status (A). TNFRSF14 expression in three datasets according to immune subtypes (B). Correlation between immune checkpoint genes and TNFRSF14 (C). The biological functions of TNFRSF14 were analyzed in metascape (D) and GSEA (E).

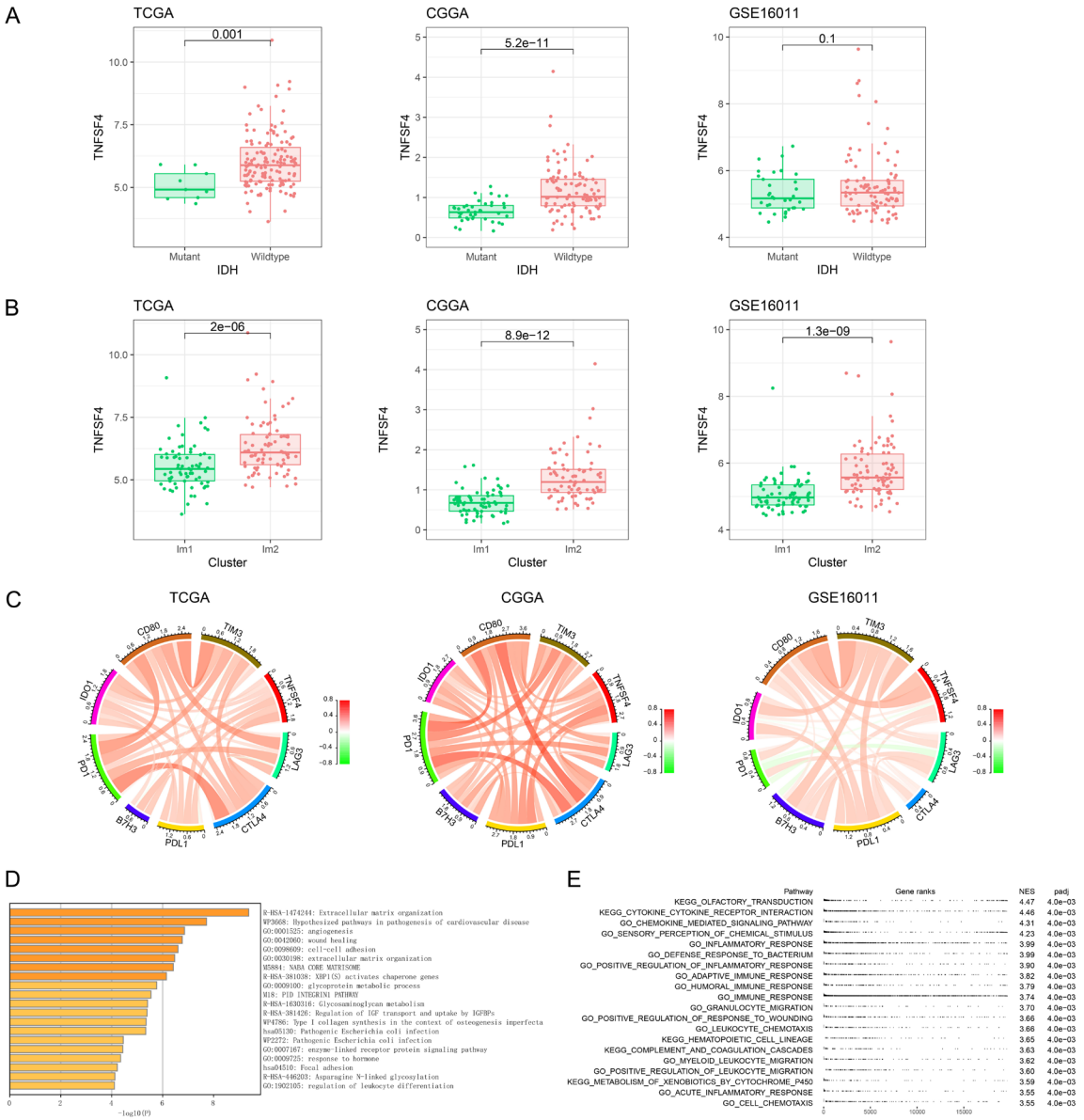

Figure S7. TNFSF4 expression in three datasets according to IDH status (A). TNFSF4 expression in three datasets according to immune subtypes (B). Correlation between immune checkpoint genes and TNFSF4 (C). The biological functions of TNFSF4 were analyzed in metascape (D) and GSEA (E).